Coordinated Model Predictive Control of Aircraft Gas Turbine Engine with Simplified Electrical System Model

Jinwoo Seok, David M. Reed, Ilya V. Kolmanovsky and Anouck R. Girard

***Abstract*— With the trends towards more electric aircraft and all electric aircraft, the electrical power requirements for aircraft have been steadily increasing, making the interactions between the electrical system and gas turbine engine significant and requiring advanced control strategies for safe and efficient operation of the aircraft. Thus, in this paper, a coordinated control strategy for a gas turbine engine, an advanced dual generator subsystem, and energy storage elements with simplified electrical bus model is developed to accommodate large transient thrust and electrical loads. The bus voltage behaviors can be regulated by imposing a power rate constraint without having additional states in the controller design. The energy storage elements assist the generators to improve system performance as well as the transient bus voltage behavior. The incorporation of energy storage elements provides the potential to extend system operation range for future more electric aircraft and all electric aircraft.**

I. Introduction

A. Motivation and Background

The electrical power requirements for aircraft have been steadily increasing over the past few decades concomitant with trends towards More Electric Aircraft (MEA) and All Electric Aircraft (AEA) [1]. A typical aircraft power system involves one or more generators connected to one or more gas turbine engines, integrated with energy storage elements that provide supplemental electrical power, a distribution system and loads. Thus, the large steady and transient electrical loads affect the operation of the subsystems such as the gas turbine engines or generators, so the interactions between the electrical system and gas turbine engine have to be addressed for safe and efficient operation of aircraft.

Consequently, our objective is to build an integrated, model-based control capability for an aircraft's propulsion and electrical power systems to accommodate large steady and transient electrical loads while maintaining the operation of the components and the overall system within a specified safe range by enforcing appropriately defined state and control constraints.

In our previous work [2], [3], an integrated control system framework is exploited using a rate-based Model Predictive Control (MPC) approach that accommodates large steady and transient electrical loads, maintains aircraft flight performance by delivering requested thrust, enforces gas turbine engine constraints, as well as electrical system constraints, and reduces fuel consumption. The advanced two-shaft distributed generator configuration is considered where one generator is connected to the High Pressure Shaft (HPS) and the other is connected to the Low Pressure Shaft (LPS) of the gas turbine engine, and energy storage elements are considered. In our previous work, the electrical bus model was not included in the overall system model, and so bus voltage requirements, such as MIL-STD-704F [4], have not been considered. This paper extends our previous work by exploiting a simplified electrical bus model to analyze the bus voltage behavior and to enforce additional constraints pertaining to the bus voltage requirements.

Jinwoo Seok is a postdoctoral research fellow in the Department of Aerospace Engineering, University of Michigan, Ann Arbor, Michigan 48109-2140. Email: sjinu@umich.edu

David M. Reed is a postdoctoral research fellow in the Department of Aerospace Engineering, University of Michigan, Ann Arbor, Michigan 48109-2140. Email: davereed@umich.edu

Ilya V. Kolmanovsky is a professor in the Department of Aerospace Engineering, University of Michigan, Ann Arbor, Michigan 48109-2140. Email: ilya@umich.edu

Anouck R. Girard is an associate professor in the Department of Aerospace Engineering, University of Michigan, Ann Arbor, Michigan 48109-2140. Email: anouck@umich.edu

B. Literature Review

The growing electrical power requirements of MEA and AEAs are indicated in [1], [5]. For instance, at least 1.6 MW will be required for a next-generation 300 pax aircraft [5]. Turboelectric propulsion requires large electrical power, so three MW generators are considered in [6] and a 40.2 MW generator is planned in [7], [8]. Furthermore, directed energy systems are one of the key 12 potential capability areas for the U.S. Air Force [9] and the electrical weapons systems rely on high electrical power density, from 0.025 to 4.5 MW depending on the type [10].

Coordinated control of an aircraft's gas turbine engine, electrical power system, and thermal management is required to accommodate these large electrical loads on aircraft, but this is challenging as discussed in [11], [12], [13], [14]. In addition to that, the challenges and possible research directions for MEA with a gas turbine engine, two-generator configuration, and battery (and/or supercapacitor) are discussed in [15]. Because of the interactions between the electrical system and the gas turbine engine system, integrated control of both systems is necessary. In [16], the significance of interactions between the gas turbine engine and the electrical system for aircraft is discussed based on the engine response when a step change reduction of electrical power occurs in the simulation. To alleviate the effects of high dynamic electrical loads on the engine, an energy storage element (supercapacitor) is exploited in [17]. In [18], a load management system for generators, contactors, buses and loads, and a battery of an aircraft is presented based on load shedding.

One of the most effective control methods with existence

Preprint submitted to 2018 American Control Conference.
Received September 18, 2017.

of constraints is MPC [19], so we employ MPC in this paper. In our previous work [2], [3], a coordinated rate-based MPC approach is developed for the control of gas turbine engine and electrical power system to track setpoints while ensuring system safety including surge margin constraints, and the focus is weighted to the gas turbine engine side. In [20], the voltage behaviors are analyzed with the gas turbine engine surge margin constraints based on high fidelity electrical system models using coordinated MPC. However, the electrical system models are confidential, so the models are not available for public domain.

In this paper, a Simulink-based Toolbox for the Modeling and Analysis of Thermodynamic Systems (T-MATS) [21], [22], [23] is used for the gas turbine engine modeling and is supplemented by an electrical power system model in Simulink. T-MATS allows one to model both steady state and dynamic gas turbine engine operation.

C. Original Contributions

- We use a simplified bus model to analyze bus voltage behaviors for coordinated control of gas turbine engine and electrical power system. By imposing power rate ($\Delta P_{busH/gen}$ and $\Delta P_{busL/gen}$) constraints one can regulate bus voltage behaviors without including bus voltage dynamics in the MPC controller, which allows us to have less complexity of the controller.
- We analyze the effects of energy storage elements to the system performance and the bus voltage behaviors. Even with small sized energy storage elements compared to the load requests, using the energy storage elements improves bus voltage behavior by reducing the constraint violations.
- We analyze the effects of different size of energy storage elements to the system. Using the larger energy storage elements is able to improve bus voltage behavior as well as overall system performance by improving tracking accuracy and reducing surge margin constraints violations that indicates the importance of advanced energy storage elements for future MEA and AEA.

D. Organization

The organization of this paper is as follows. Section II describes plant models and linear prediction model. Section III formulates the problem and Section IV addresses the control design. Section V presents the primary simulation results and finally, Section VI presents our conclusions.

II. Modeling

In this paper, we focus on describing the simplified electrical bus model, while the details of other subsystem models can be found in [3]. In this section, models of the gas turbine engine, generators, energy storage elements, and a simplified bus model are described assuming the dynamics of the electrical system are much faster than the dynamics of the gas turbine engine. The system architecture is shown in Fig. 1.

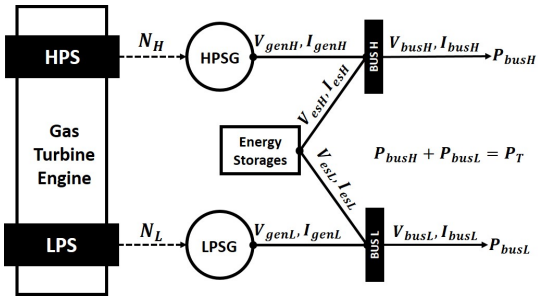

Fig. 1: Overall system architecture.

Each of two generators is attached to the each of the HPS and LPS of gas turbine engine. Each generator is connected to its own bus and the energy storage elements are connected to both buses, so we have two bus voltages to consider. Consequently, the total electrical power is the sum of the electrical powers of both buses.

A. Gas Turbine Engine

The JT9D gas turbine engine model provided with T-MATS package [22] is used to represent engine dynamics. T-MATS is a Simulink-based tool for thermodynamic system simulation developed and released by NASA to facilitate research involving gas turbine engine simulations and control of the kind pursued in this paper.

B. Generators

The two generators are each connected to different shafts of the gas turbine engine: one to the HPS and one to the LPS. We refer to the generator that is connected to the HPS as the High Pressure Shaft Generator (HPSG) and the generator that is connected to the LPS as the Low Pressure Shaft Generator (LPSG). Assuming that the dynamics of the generators are much faster than those of the gas turbine engine [24], a simple relationship between the shaft speeds of the gas turbine engine and the output power of the generators is adopted based on given efficiencies of the generators; thus, given electrical power outputs of the generators, the torques that the generators create on the gas turbine engine shafts can be computed according to

$$\tau_{E_H} = \frac{P_{genH}}{N_H \times \eta_H}, \quad \tau_{E_L} = \frac{P_{genL}}{N_L \times \eta_L}, \tag{1}$$

where P_{genH}, N_H, τ_{E_H} and η_H are, respectively, HPSG output power, the shaft speed, torque on the shaft and efficiency of the HPSG, and P_{genL}, N_L, τ_{E_L} and η_L are, respectively, LPSG output power, the shaft speed, torque on the shaft and efficiency of the LPSG. Note that the above electrical power system representation is suitable given the specific control objectives in this paper and is justified by the time-scale separation between the engine dynamics and the dynamics in the electrical power system. In the subsequent analysis and simulations, constant values of the efficiencies, $\eta_H = \eta_L = 0.9$, are assumed.

Preprint submitted to 2018 American Control Conference.
Received September 18, 2017.

C. Energy Storage Elements

The energy storage element model is as follows:

$$\frac{dE_j}{dt} = -P_j, \tag{2}$$

where E_j is the total energy stored in the energy storage j, P_j is power to/from the energy storage j, and j indicates the type of energy storage element. In this paper, a battery and/or ultracapacitor are exploited as the energy storage elements, so $j \in \{B, C\}$ where B indicates the battery and C indicates the ultracapacitor. Then, the State of Charge (SoC) is given by

$$SoC_j = \frac{E_j}{E_{j_{Max}}}, \tag{3}$$

where $E_{j_{Max}}$ is the maximum energy that can be stored in the energy storage j.

D. Simplified Bus Model with Constant Power Load

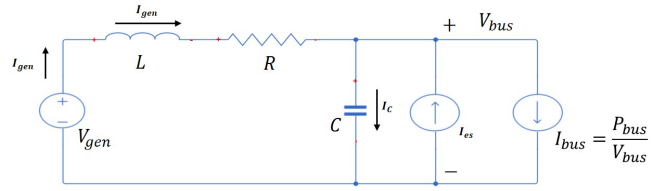

Fig. 2: Simplified electrical model.

In this section, we introduce the simplified electrical system model, depicted in Fig. 2, that allows us to analyze the bus voltage behavior. While simplified, the level of complexity in this constant power bus model is suitable for our purpose. Additionally, we note that constant power loads are commonly used to represent power electronics loads [25], [26], that can have a destabilizing effect due to their negative effective resistance.

P_{bus} is the power load at the bus, assumed to be constant. Then,

$$V_{bus} = V_{gen} - L\frac{dI_{gen}}{dt} - RI_{gen}, \tag{4}$$

where V_{bus} is bus voltage (load voltage), V_{gen} is generator voltage, L is a constant value of the inductor, R is a constant value of the resistor, and I_{gen} is current from the generator as follows,

$$I_{gen} = I_c + I_{bus} - I_{es} = C\frac{dV_{bus}}{dt} + \frac{P_{bus}}{V_{bus}} - I_{es}, \tag{5}$$

where I_c is the current through the capacitor, I_{bus} is the current on the bus, I_{es} is current from energy storage elements, and C is a constant value of the capacitor. Substituting (5) into (4) yields

$$\begin{aligned} V_{bus} =& V_{gen} - L\frac{d}{dt}\left(C\frac{dV_{bus}}{dt} + \frac{P_{bus}}{V_{bus}} - I_{es}\right) \\ & - R\left(C\frac{dV_{bus}}{dt} + \frac{P_{bus}}{V_{bus}} - I_{es}\right). \end{aligned} \tag{6}$$

Consequently, we have the following form,

$$\begin{aligned} & V_{bus} - V_{gen} + LC\ddot{V}_{bus} + LP_{bus}\left(\frac{-\dot{V}_{bus}}{V_{bus}^2}\right) \\ & \qquad + L\dot{I}_{es} + RC\dot{V}_{bus} + \frac{RP_{bus}}{V_{bus}} + RI_{es} = 0, \\ \implies & LC\ddot{V}_{bus} + \left(RC - \frac{LP_{bus}}{V_{bus}^2}\right)\dot{V}_{bus} + L\dot{I}_{es} \\ & \qquad + V_{bus} - V_{gen} + \frac{RP_{bus}}{V_{bus}} + RI_{es} = 0. \end{aligned} \tag{7}$$

Given the R, $V_{gen,0}$ and $P_{bus,0}$, the initial bus voltage, $V_{bus,0}$, can be obtained by solving the following equation,

$$\begin{aligned} & V_{bus,0} + \frac{RP_{bus,0}}{V_{bus,0}} = V_{gen,0} \\ \implies & -V_{bus,0}^2 + V_{gen,0}V_{bus,0} = RP_{bus,0}. \end{aligned} \tag{8}$$

Given L, R, C, V_{gen}, I_{es}, and P_{bus}, the bus voltage, V_{bus} is computed based on (7) and then, I_{gen} is computed based on (5).

We assume that $V_{es} = V_{bus}$ and the dynamics of the generator are fast enough to supply the required voltage to maintain the bus voltage. Thus, a PI feedback loop maintains the bus voltage as a constant value (540 DCV) by adjusting the generator voltage. The overall bus model diagram is shown in Fig. 3.

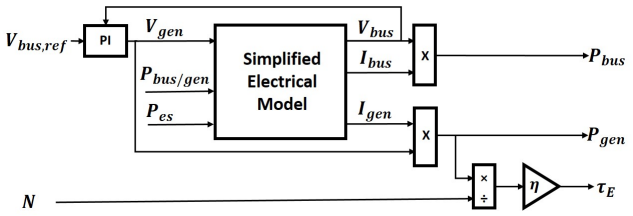

Fig. 3: Overall bus model diagram.

The portion of the electrical power at the bus coming from the generator ($P_{bus/gen}$), power from the energy storage elements (P_{es}) and generator voltage (V_{gen}) yield the bus voltage (V_{bus}) and current on the bus (I_{bus}). The PI loop picks V_{gen} to maintain V_{bus} to a constant setpoint ($V_{bus,ref}$ = 540 V). The electrical power output of the bus (P_{bus}) is computed by $V_{bus} \times I_{bus}$. The generator power output (P_{gen}) is computed by $V_{gen} \times I_{gen}$. Then, the electrical torque (τ_E) on the gas turbine engine is determined by dividing P_{gen} by the shaft speed (N) of the gas turbine engine then multiplying by the efficiency (η).

Finally, we note that the electrical parameters, $C = 42mF$, $R = 92mS$, and $L = \frac{1}{w_n^2 \times C} = 41.88\mu H$ where $w_n = 2 \times \pi \times 120$, have been selected to mimic the transient bus voltage response of more detailed electrical system models [20] and are similar to those used in other studies [26].

E. Linear Design Model

We use the linear prediction model in [3] for the MPC controller, so details of linear prediction model can be found

Preprint submitted to 2018 American Control Conference.
Received September 18, 2017.

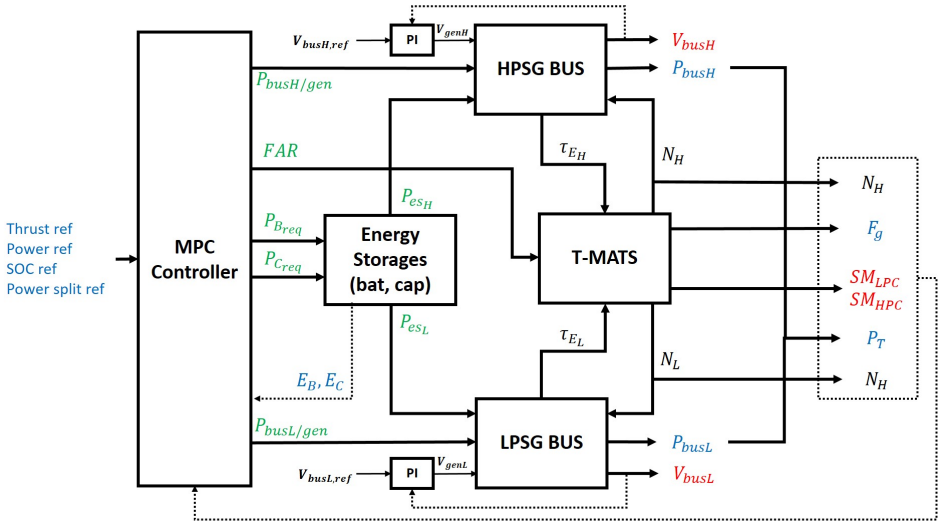

Fig. 4: Overall system diagram.

in [3]. Note that the bus models (states of bus voltages) are not included in the linear prediction model, instead we impose constraints on $\Delta P_{busH/gen}$ and $\Delta P_{busL/gen}$ to regulate the bus voltage behaviors that allows us to have less complexity of the controller.

III. Problem Formulation

Given a gas turbine engine, energy storage elements, the simplified electrical model with two generators, one connected to each shaft of the gas turbine engine, a requested thrust level and (large) expected/requested electrical loads, determine the fuel to air ratio of the gas turbine engine, input/output power of the energy storage elements and the electrical power output of each generator to supply all the required electrical loads, maintain the requested thrust level, and minimize fuel consumption, subject to surge margin limits, bus voltage requirements, and other constraints.

IV. Controller Design

A. Overall Architecture

The overall system diagram is shown in Fig. 4. One generator is attached to the each of the HPS and LPS of the T-MATS engine. Each generator is connected to its own bus and the energy storage elements are connected to both buses. Then, the total electrical power of the system (P_T) is the sum of the power output from the HPSG bus (P_{busH}) and power output from the LPSG bus (P_{busL}).

The MPC controller generates five input signals based on thrust, power, SoC, power split references and feedback signals: fuel to air ratio (FAR), required portion of the electrical power coming from the HPSG at the HPSG bus ($P_{busH/gen}$), required portion of the electrical power coming from the LPSG at the LPSG bus ($P_{busL/gen}$), required power from the battery ($P_{B_{req}}$), and required power from the ultracapacitor ($P_{C_{req}}$). The electrical power from energy storage elements is split to HPSG bus (P_{esH}) and LPSG bus (P_{esL}). The thrust (F_g) should follow the thrust reference, the total electrical power output (P_t) should follow the power reference, the energy level of each of battery and ultracapacitor (E_B and E_C) should follow the SOC reference, and the power split between the two generators should follow the power split reference. In addition to that, HPC and LPC surge margins (SM_{HPC} and SM_{LPC}) have to satisfy the constraints, and HPSG and LPSG bus voltages (V_{busH} and V_{busL}) have to satisfy the requirements.

B. Optimal Power Split

The optimal power split between the two generator considers the fuel efficiency and surge margin constraints. The offline optimal power split map decides the power split between the LPSG and HPSG based on the current thrust level and total electrical power request. The details can be found in our previous work [3].

C. Energy Storage Elements Control Strategy

The energy storage SoC is soft constrained between 40% and 60%. The setpoint for the energy storage SoC is changed according to the following rule-based strategy:

- When thrust and load are decreased: track high SoC setpoint, which is 90% in our simulation case study – charge.
- When thrust and load are increased: track low SoC setpoint, which is 10% in our simulation case study – supply.
- When one is decreased and the other is maintained: track high SoC setpoint – charge.
- When one is increased and the other is maintained: track low SoC setpoint – supply.
- All other cases: track the setpoint corresponding to the mid-range between lower and upper limit – maintain desired SoC.

The basic idea behind these rules is to charge the energy storage if extra power is available, and discharge the energy storage if extra power is needed.

Preprint submitted to 2018 American Control Conference.
Received September 18, 2017.

The power split from energy storage elements to each bus is based on the ratio of $P_{busH/gen}$ and $P_{busL/gen}$. The power split ratio is defined as follows:

$$\lambda_{es} = \frac{P_{busH/gen}}{P_{busL/gen}} = \frac{P_{esH}}{P_{esL}}. \quad (9)$$

The power split ratio, λ_{es}, determines the power from the battery and the ultracapacitor to each bus.

D. Rate-based MPC Controller Design

1) Scaled Model: To alleviate the effects of different order of magnitudes of the inputs and outputs for the MPC controller, the inputs and outputs of the linear model are scaled before controller design. We want to scale the inputs and outputs such that the maximum value of each element in the scaled inputs and outputs is one. The details can be found in [3].

2) Offset State: The nominal linear discrete-time model can be augmented with extra offset states to compensate for errors between linear model predictions and the response of the actual nonlinear system. Then, the offset state is defined by difference between the actual nonlinear model and linearized model assuming the measurements or accurate estimates are available. The details can be found in [3].

3) Rate-based MPC: The design process of the rate-based MPC controller is now described. The states of the linear model used for prediction are assumed to be available from measurements and appropriately designed estimators. The rate-based MPC design described in this section is for the system configuration with two energy storage elements and two surge margin offset states. Other system configurations are handled similarly.

The discrete-time model is obtained using a sampling period of 0.01 sec based on the scaled input-output model. A rate-based MPC controller can be designed to perform setpoint tracking based on the discrete-time prediction model shown, without extra offset states, as

$$\delta x_{k+1} = A_d \delta x_k + B_d \delta u_k, \quad \delta y_k = C_d \delta x_k + D_d \delta u_k, \quad (10)$$

where k indicates discrete time instant, $A_d^{7\times7}$, $B_d^{7\times5}$, $C_d^{6\times7}$, $D_d^{6\times5}$, and δy_k = $[\delta F_g \ \delta P_T \ \delta P_D \ \delta P_D \ E_B \ E_C]^T$. The states vector δx_k, is $[\delta x_{N_H} \ \delta x_{N_L} \ \delta x_{Fg} \ \delta x_{SM_{LPC}} \ \delta x_{SM_{HPC}} \ E_B \ E_C]^T$ where δx_{N_H} is the HPS speed deviation, δx_{N_L} is the LPS speed deviation, δx_{Fg} is the thrust deviation, $\delta x_{SM_{LPC}}$ is the LPC surge margin deviation, $\delta x_{SM_{HPC}}$ is the HPC surge margin deviation, E_B is battery energy, and E_C is ultracapacitor energy. The inputs vector δu_k is $[\delta FAR \ \delta P_{busH/gen} \ \delta P_{busL/gen} \ \delta P_{Breq} \ \delta P_{Creq}]^T$, and contains the deviations in the respective inputs.

The control objective is to follow a requested command (setpoint) r where $r = [\delta Fg_{req} \ \delta P_{Treq} \ \delta P_{Dreq_{max}} \ \delta P_{Dreq_{min}} \ E_{Bd} \ E_{Cd}]^T$, that is, follow thrust requests, total electrical power requests, optimal maximum power difference requests, optimal minimum power difference requests, stored battery energy requests, and stored ultracapacitor energy requests, respectively. Then, the state and control increments are defined as

$$\Delta x_k = \delta x_{k+1} - \delta x_k, \quad \Delta u_k = \delta u_{k+1} - \delta u_k, \quad (11)$$

and the error between outputs (y_k) and setpoints (r) is defined as

$$e_k = C_d \delta x_k + D_d \delta u_k - r. \quad (12)$$

Then,

$$\begin{aligned} \Delta x_{k+1} &= A_d \Delta x_k + B_d \Delta u_k, \\ e_{k+1} &= C_d \Delta x_k + D_d \Delta u_k + e_k, \\ \delta x_{k+1} &= \delta x_k + \Delta x_k, \\ \delta u_{k+1} &= \delta u_k + \Delta u_k. \end{aligned} \quad (13)$$

Equation (13) can be extended with two surge margin offset states and two compensated surge margin states. The extended linear prediction model is as follows:

$$\begin{aligned} \Delta x_{k+1} &= A_d \Delta x_k + B_d \Delta u_k, \\ e_{k+1} &= C_d \Delta x_k + D_d \Delta u_k + e_k, \\ \delta x_{k+1} &= \delta x_k + \Delta x_k, \\ \delta u_{k+1} &= \delta u_k + \Delta u_k, \\ d_{k+1} &= d_k, \\ \delta \bar{x}_{k+1} &= F \delta x_k + d_k, \end{aligned} \quad (14)$$

where d_k is the 2×1 surge margin offset states vector, $\delta \bar{x}_{k+1}$ is the 2×1 compensated surge margin deviations vector, and $F = [0_{2\times3} \ \ I_{2\times2} \ \ 0_{2\times2}]$. The cost function to be minimized is given by

$$J_N = \sum_{k=0}^{N-1} e_{k|t}^T Q e_{k|t} + \Delta u_{k|t}^T R \Delta u_{k|t},$$

subject to the constraints:

$$\begin{aligned} &\delta x_{min} \le \delta x_{k|t} \le \delta x_{max}, \quad k = 0, \cdots, N, \\ &\delta u_{min} \le \delta u_{k|t} \le \delta u_{max}, \quad k = 0, \cdots, N-1, \\ &\Delta u_{min} \le \Delta u_{k|t} \le \Delta u_{max}, \quad k = 0, \cdots, N-1, \end{aligned} \quad (15)$$

where N is the prediction horizon, Q is a 6×6 diagonal weight matrix associated with the six errors, R is a 5×5 diagonal weight matrix associated with the five inputs, $e_{k|t}$ is the predicted error k steps ahead when the prediction is made at time instant t, $\delta u_{k|t}$ is is the predicted input k steps ahead when the prediction is made at time instant t, δx_{min} and δx_{max} designate state bounds, and $\delta u_{min}, \delta u_{max}, \Delta u_{min}$ and Δu_{max} designate the bounds on the control inputs and their time rates of change.

Note that the cost function is constructed to penalize the deviation of power difference between the two generators (P_D) from the maximum power difference setpoint ($P_{Dreq_{max}}$) and the minimum power difference setpoint ($P_{Dreq_{min}}$), where these setpoints are computed from optimal power split ranges. The same weights are used for both tracking errors. This strategy maintains P_D in between the two setpoints and hence within/in the middle of the optimal power split range.

Preprint submitted to 2018 American Control Conference.
Received September 18, 2017.

The above tracking MPC formulation can be re-written as a standard MPC problem (to which standard MPC solvers are applicable) for an extended system with a larger state vector,

$$x_{k|t}^{ext} = \begin{bmatrix} \Delta x_{k|t}^T & e_{k|t}^T & \delta x_{k|t}^T & \delta u_{k|t}^T & d_{k|t}^T & \delta \bar{x}_{k|t}^T \end{bmatrix}^T, \quad (16)$$

and the extended state prediction model given by

$$x_{k+1|t}^{ext} = \begin{bmatrix} A_d & 0 & 0 & 0 & 0 & 0 \\ C_d & I_{6\times 6} & 0 & 0 & 0 & 0 \\ I_{7\times 7} & 0 & I_{7\times 7} & 0 & 0 & 0 \\ 0 & 0 & 0 & I_{5\times 5} & 0 & 0 \\ 0 & 0 & 0 & 0 & I_{2\times 2} & 0 \\ 0 & 0 & F & 0 & I_{2\times 2} & 0 \end{bmatrix} x_{k|t}^{ext} + \begin{bmatrix} B_d \\ D_d \\ 0 \\ I_{4\times 4} \\ 0 \\ 0 \end{bmatrix} \Delta u_{k|t}. \quad (17)$$

For this extended system, the state penalty matrix has the form

$$Q_{ext} = \begin{bmatrix} 0 & 0 & 0 & 0 & 0 & 0 \\ 0 & Q & 0 & 0 & 0 & 0 \\ 0 & 0 & 0 & 0 & 0 & 0 \\ 0 & 0 & 0 & 0 & 0 & 0 \\ 0 & 0 & 0 & 0 & 0 & 0 \\ 0 & 0 & 0 & 0 & 0 & 0 \end{bmatrix}, \quad (18)$$

and the control penalty matrix is $R_{ext} = R$. The prediction horizon, N=30 and sampling period of 0.01 sec are considered.

The qpOASES (quadratic problem Online Active Set Strategy) [27] is used to solve Quadratic Problem (QP) for the rate-based MPC controller. To improve the computation time for the QP solver, a warm start strategy is adopted.

Note that the states of the bus voltages are not included in the linear prediction model for the rate-based MPC controller, but the power rate constraints are imposed to regulate the bus voltage behaviors that allows us to have less complexity of the rate-based MPC controller while yielding good bus voltage regulating performance as shown in the simulation results. Since the power rate constraints limit the amount of electrical power from the generator, the required electrical power may not be supplied instantly, so load shedding may be necessary. The power rate constraints are $\Delta P_{busH/gen} = \Delta P_{busL/gen} = \pm 200$ [kW].

V. Simulations and Results

In this section, different cases are simulated to verify the effectiveness of the power rate constraints for regulating bus voltage behaviors and the benefits of the energy storage elements for the system. To these ends, we design thrust and electrical power request profiles that contain large step changes of thrust or electrical power, and combinations thereof.

The performance metrics are: the total fuel consumption, w_f, the average thrust deviation from the setpoint, Fg_{AvgDev}, the average total electrical power deviation from the setpoint, $P_{T_{AvgDev}}$, the number of surge margin violations, n_{smv}, the duration of the i^{th} surge margin violation, $t_{d_{smv}}^i$, and the maximum amount of the i^{th} surge margin violation, SM_{MaxV}^i. More details on the performance metrics can be found in [3].

A. Electrical Power Rate Constraints

The cases without and with the electrical power rate constraints are compared to verify the effectiveness of power rate constraints for regulating bus voltage behaviors. Note that both cases do not include the energy storage elements. The system responses are compared in Fig. 5.

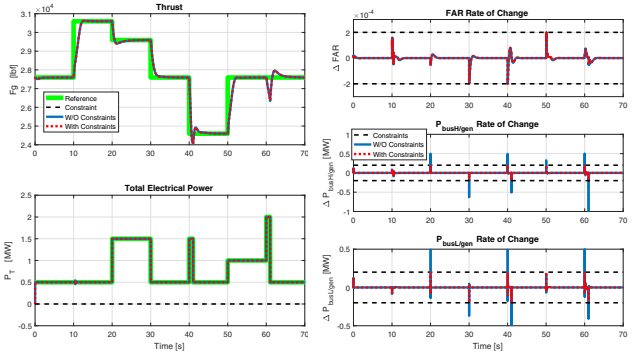

Fig. 5: Comparison of the cases with and without electrical power rate constraints: thrust and total electrical power trackings (left), FAR and power rate (right).

As observed, both cases yield similar thrust and electrical power tracking, but actually, the case of without power rate constraints yields better total electrical power tracking as indicated by $P_{T_{AvgDev}}$ in Table I because the case of without power rate constraints is not limited by $\Delta P_{busH/gen}$ and $\Delta P_{busL/gen}$ constraints as shown in the right subfigures of Fig. 5, so the electrical power is promptly supplied without the limitations. However, the bus voltage requirements have to be considered. The bus voltage behaviors between 20 to 20.2 sec and 61 to 61.2 sec are shown in Fig. 6.

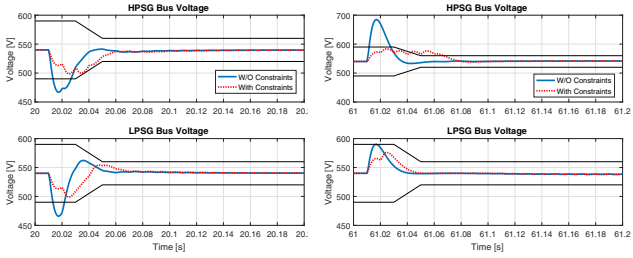

Fig. 6: Comparison of bus voltage behaviors of the cases with and without electrical power rate constraints.

The bus voltage requirements as shown in black solid lines in Fig. 6 are determined based on the military specifications for 270 V aircraft power subsystems [4]. As observed, the case of without power rate constraints easily violates the bus voltage requirements while the case of with power rate constraints does not; that implies the power rate constraints successfully regulate the bus voltage behaviors to meet the requirements. However, at the extreme situation (very large short period electrical power request with constant thrust level), as shown in HPSG bus between 61 to 61.2 sec in

Preprint submitted to 2018 American Control Conference.
Received September 18, 2017.

TABLE I: Performance metrics comparison.

		W/O constraints	W/O ES	With ES	With Large ES
W_f	[Kg]	65.62	65.62	65.64	65.60
Fg_{AvgDev}	[lbf]	154.21	154.51	152.28	133.13
$P_{T_{AvgDev}}$	[KW]	2.0859	3.0632	2.3448	2.1151
n_{smv}	[times]	3	3	3	2
$t_{d_{smv}}$	[s]	1.81 / 1.33 / 0.94	1.81 / 1.33 / 0.95	1.71 / 1.16 / 0.92	1.58 / 0.73
SM_{MaxV}	[%]	0.99 / 1.59 / 2.60	0.99 / 1.59 / 2.63	0.95 / 1.20 / 2.25	0.82 / 0.80

Fig. 6, the case of with power rate constraints also slightly violates the bus voltage requirements. This implies the need of energy storage elements for the extreme situations to extend system operation ranges.

B. Energy Storage Elements

Thus, the cases without and with energy storage elements (battery-capacitor pack) are compared to verify the benefits of the energy storage elements to the system operations including the bus voltage behaviors. Note that the size of the energy storage element is relatively small compared to our load request. The detailed specifications of the energy storage element can be found in [3]. The system responses are compared in Fig. 7.

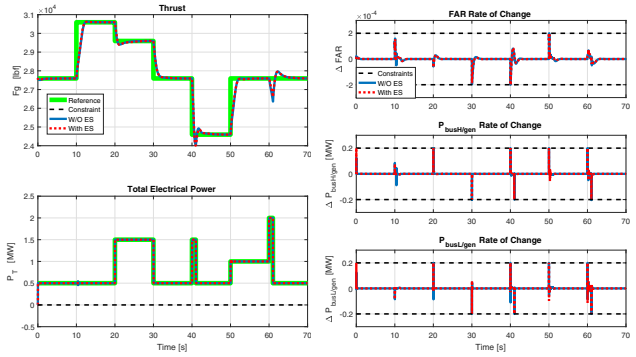

Fig. 7: Comparison of the cases with and without energy storage elements: thrust and total electrical power tracking (left), FAR and power rates (right).

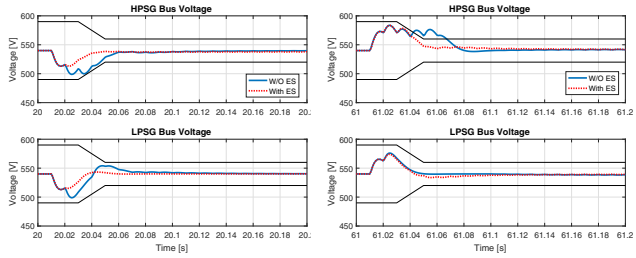

Fig. 8: Comparison of bus voltage behaviors of the cases with and without energy storage elements.

As expected, both cases satisfy the $\Delta P_{busH/gen}$ and $\Delta P_{busL/gen}$ constraints, but the case of with energy storage elements yields better thrust tracking and electrical power tracking as observed in Fig. 7 and indicated by Fg_{AvgDev} and $P_{T_{AvgDev}}$ in Table I because the energy storage elements assist the generator. The bus voltage behaviors between 20 to 20.2 sec and 61 to 61.2 sec are shown in Fig. 6.

As observed, the case of with energy storage element does not violate the bus voltage requirements even in the extreme situation, and improves the overall bus voltage behaviors. However, with the existence of large loads, the surge margin constrains are sometimes violated with a maximum of 2.25% as shown in Table I.

C. Large Energy Storage Elements

Thus, the case of larger energy storage elements (10 times larger battery and 10 times larger ultracapacitor) is compared with the case of original energy storage elements to investigate the benefits of the larger size of the energy storage elements to the system operations as well as the voltage behaviors. The system responses are compared in Fig. 9.

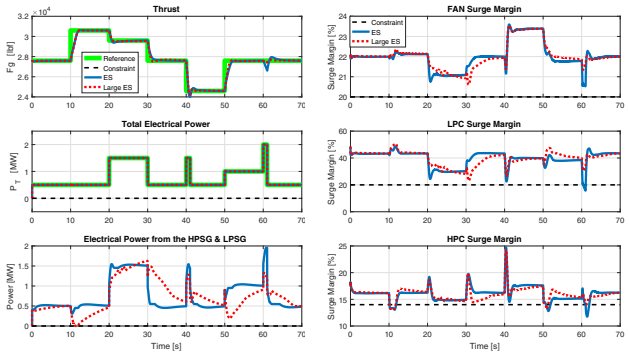

Fig. 9: Comparison of the cases of the different sizes of the energy storage elements: thrust and total electrical power tracking, electrical power from the generators (left), surge margins (right).

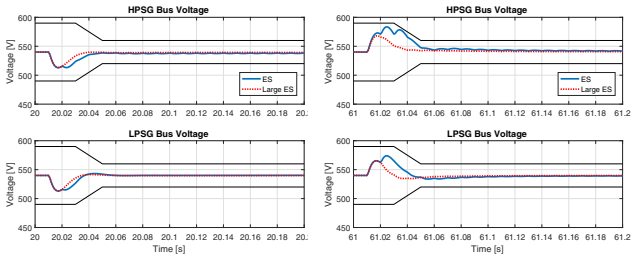

Fig. 10: Comparison of bus voltage behaviors of the cases of the different sizes of energy storage elements.

Because the electrical power from the generators side is reduced in high load situations for the case of with larger energy storage elements, it yields better thrust tracking and electrical power tracking as observed in Fig. 9 and indicated by Fg_{AvgDev} and $P_{T_{AvgDev}}$ in Table I. In addition to that, the case of with larger energy storage elements reduces the number and magnitude of the surge margin violations which implies safer operations.

The bus voltage behaviors between 20 to 20.2 sec and 61 to 61.2 sec are shown in Fig. 10. As expected, the case of with larger energy storage elements yields better bus voltage behaviors which implies the system can handle more loads.

VI. Conclusions

In this paper, a coordinated control strategy for a gas turbine engine, an advanced dual generator subsystem, and energy storage elements with simplified electrical bus model for MEA and AEA is developed to accommodate large transient thrust and electrical loads. Especially, the simplified electrical bus model is exploited and the bus voltage behaviors as well as the system operations are analyzed for different cases: with and without power rate constraints, with and without energy storage elements, and different sizes of the energy storage elements. The single rate-based MPC design is exploited for the entire simulated operating range.

The simulation results indicate that without including bus voltage dynamics in the MPC controller, voltage behaviors can be regulated to satisfy the bus voltage requirements by imposing power rate ($\Delta P_{busH/gen}$ and $\Delta P_{busL/gen}$) constraints. The energy storage elements assist the system to have better bus voltage behaviors that reduces the bus voltage requirements violations as well as better setpoints tracking. The larger energy storage elements improve the overall performance of the system that promises potential of system operation ranges extensions, so the advanced energy storage elements are one of the important subsystems for the future MEA and AEA.

References

[1] I. Moir and A. Seabridge, *Aircraft Systems: Mechanical, Electrical and Avionics Subsystems Integration*, 3rd ed. Wiley, 2008.

[2] J. Seok, I. Kolmanovsky, and A. Girard, "Integrated/coordinated control of aircraft gas turbine engine and electrical power system: Towards large electrical load handling," in *IEEE Conference on Decision and Control*, Dec 2016, pp. 3183–3189.

[3] J. Seok, I. V. Kolmanovsky, and A. R. Girard, "Coordinated model predictive control of aircraft gas turbine engine and power system," *Journal of Guidance, Control, and Dynamics*, vol. 40, no. 10, pp. 2538 – 2555, 2017.

[4] *MIL-STD-704F, Aircraft Electric Power Characteristics*, Department of Defense, Mar 2004.

[5] J. A. Rosero, J. A. Ortega, E. Aldabas, and L. Romeral, "Moving towards a more electric aircraft," *IEEE Aerospace and Electronic Systems Magazine*, vol. 22, pp. 3–9, Mar 2007.

[6] C. A. Luongo, P. J. Masson, T. Nam, D. Mavris, H. D. Kim, G. V. Brown, M. Waters, and D. Hall, "Next generation more-electric aircraft: A potential application for hts superconductors," *IEEE Transactions on Applied Superconductivity*, vol. 19, pp. 1055–1068, Jun 2009.

[7] J. Felder, H. Kim, and G. Brown, "Turboelectric distributed propulsion engine cycle analysis for hybrid-wing-body aircraft," in *AIAA Aerospace Sciences Meeting including The New Horizons Forum and Aerospace Exposition*, Jan 2009.

[8] H. D. Kim, "Distributed propulsion vehicles," in *27th International Congress of the Aeronautical Sciences*, Sep 2010.

[9] U. S. A. F. C. Scientist, "Technology horizons: A vision for air force science and technology 2010-30," United States Air Force, Tech. Rep., 2010.

[10] I. R. McNab, "Pulsed power for electric guns," *IEEE Transactions on Magnetics*, vol. 33, pp. 453–460, Jan 1997.

[11] A. Behbahani, D. Culley, S. Garg, R. Millar, B. Smith, J. Wood, T. Mahoney, R. Quinn, S. Carpenter, B. Mailander *et al.*, "Status, vision, and challenges of an intelligent distributed engine control architecture," *SAE Technical Paper 2007-01-3859*, 2007.

[12] A. R. Behbahani, A. Von Moll, R. Zeller, and J. Ordo, "Aircraft integration challenges and opportunities for distributed intelligent control, power, thermal management, diagnostic and prognostic systems," *SAE Technical Paper 2014-01-2161*, 2014.

[13] J. S. Litt, D. L. Simon, S. Garg, T.-H. Guo, C. Mercer, R. Millar, A. Behbahani, A. Bajwa, and D. T. Jensen, "A survey of intelligent control and health management technologies for aircraft propulsion systems," *Journal of Aerospace Computing, Information, and Communication*, vol. 1, no. 12, pp. 543–563, 2004.

[14] M. P. DeSimio, B. M. Hencey, and A. C. Parry, "Online prognostics for fuel thermal management system," in *ASME 2015 Dynamic Systems and Control Conference*. American Society of Mechanical Engineers, Oct 2015, p. V001T08A003.

[15] P. Rakhra, P. J. Norman, S. J. Galloway, and G. M. Burt, "Modelling and simulation of a mea twin generator uav electrical power system," in *International Proceedings of Universities' Power Engineering Conference*, Sep 2011, pp. 1–5.

[16] P. J. Norman, S. J. Galloway, G. M. Burt, J. E. Hill, and D. R. Trainer, "Evaluation of the dynamic interactions between aircraft gas turbine engine and electrical system," in *IET Conference on Power Electronics, Machines and Drives*, Apr 2008, pp. 671–675.

[17] R. Todd, D. Wu, J. A. dos Santos Girio, M. Poucand, and A. J. Forsyth, "Supercapacitor-based energy management for future aircraft systems," in *Applied Power Electronics Conference and Exposition*, Feb 2010, pp. 1306–1312.

[18] B. Shahsavari, M. Maasoumy, A. Sangiovanni-Vincentelli, and R. Horowitz, "Stochastic model predictive control design for load management system of aircraft electrical power distribution," in *American Control Conference*, Jul 2015, pp. 3649–3655.

[19] J. Rawlings and D. Mayne, *Model Predictive Control: Theory and Design*, 1st ed. Nob Hill Publishing, 2009.

[20] W. Dunham, B. Hencey, I. Kolmanovsky, and A. Girard, "Predictive propulsion and power control for large transient power loads in a more electric aircraft," in *American Control Conference*, May 2017, pp. 4055–4061.

[21] J. W. Chapman, T. M. Lavelle, J. S. Litt, R. D. May, and T.-H. Guo, "Propulsion system simulation using the toolbox for the modeling and analysis of thermodynamic systems (t-mats)," in *Propulsion and Energy Forum*, Jul 2014.

[22] A. Zinnecker, J. W. Chapman, T. M. Lavelle, and J. S. Litt, "Development of a twin-spool turbofan engine simulation using the toolbox for modeling and analysis of thermodynamic systems (t-mats)," in *Propulsion and Energy Forum*, Jul 2014.

[23] J. W. Chapman, T. M. Lavelle, J. S. Litt, and T.-H. Guo, "A process for the creation of t-mats propulsion system models from npss data," in *Propulsion and Energy Forum*, Jul 2014.

[24] M. Corbett, P. Lamm, J. McNichols, M. Boyd, and M. Wolff, "Effects of transient power extraction on an integrated hardware-in-the-loop aircraft/propulsion/power system," *SAE Technical Paper 2008-01-2926*, 2008.

[25] G. Sulligoi, D. Bosich, G. Giadrossi, L. Zhu, M. Cupelli, and A. Monti, "Multiconverter medium voltage dc power systems on ships: Constant-power loads instability solution using linearization via state feedback control," *IEEE Transactions on Smart Grid*, vol. 5, no. 5, pp. 2543 – 2552, 2014.

[26] P. Karlsson and J. Svensson, "Dc bus voltage control for a distributed power system," *IEEE Transactions on Power Electronics*, vol. 18, no. 6, pp. 1405 – 1412, 2003.

[27] H. Ferreau, C. Kirches, A. Potschka, H. Bock, and M. Diehl, "qpOASES: A parametric active-set algorithm for quadratic programming," pp. 327–363, 2014.